AMERICAN SOCIETY FOR MICROBIOLOGY | mBio®

RESEARCH ARTICLE

Postinfluenza Environment Reduces *Aspergillus fumigatus* Conidium Clearance and Facilitates Invasive Aspergillosis *In Vivo*

Ko-Wei Liu,[a] Madeleine S. Grau,[a] Jane T. Jones,[a] Xi Wang,[a] Elisa M. Vesely,[a] Matthew R. James,[a] Cecilia Gutierrez-Perez,[a] Robert A. Cramer,[a] Joshua J. Obar[a]

[a]Department of Microbiology and Immunology, Geisel School of Medicine at Dartmouth, Hanover, New Hampshire, USA

ABSTRACT *Aspergillus fumigatus* is a human fungal pathogen that is most often avirulent in immunecompetent individuals because the innate immune system is efficient at eliminating fungal conidia. However, recent clinical observations have shown that severe influenza A virus (IAV) infection can lead to secondary *A. fumigatus* infections with high mortality. Little is currently known about how IAV infection alters the innate antifungal immune response. Here, we established a murine model of IAV-induced *A. fumigatus* (IAV-*Af*) superinfection by inoculating mice with IAV followed 6 days later by *A. fumigatus* conidia challenge. We observed increased mortality in the IAV-*Af*-superinfected mice compared to mice challenged with either IAV or *A. fumigatus* alone. *A. fumigatus* conidia were able to germinate and establish a biofilm in the lungs of the IAV-*Af* superinfection group, which was not seen following fungal challenge alone. While we did not observe any differences in inflammatory cell recruitment in the IAV-*Af* superinfection group compared to single-infection controls, we observed defects in *Aspergillus* conidial uptake and killing by both neutrophils and monocytes after IAV infection. pHrodo Green zymosan bioparticle (pHrodo-zymosan) and CM-H2DCFDA [5-(and-6)-chloromethyl-2′,7′-dichlorodihydrofluorescein diacetate] staining, indicators of phagolysosome maturation and reactive oxygen species (ROS) production, respectively, revealed that the fungal killing defect was due in part to reduced phagolysosome maturation. Collectively, our data demonstrate that the ability of neutrophils and monocytes to kill and clear *Aspergillus* conidia is strongly reduced in the pulmonary environment of an IAV-infected lung, which leads to invasive pulmonary aspergillosis and increased overall mortality in our mouse model, recapitulating what is observed clinically in humans.

IMPORTANCE Influenza A virus (IAV) is a common respiratory virus that causes seasonal illness in humans, but can cause pandemics and severe infection in certain patients. Since the emergence of the 2009 H1N1 pandemic strains, there has been an increase in clinical reports of IAV-infected patients in the intensive care unit (ICU) developing secondary pulmonary aspergillosis. These cases of flu-*Aspergillus* superinfections are associated with worse clinical outcomes than secondary bacterial infections in the setting of IAV. To date, we have a limited understanding of the cause(s) of secondary fungal infections in immunocompetent hosts. IAV-induced modulation of cytokine production and innate immune cellular function generates a unique immune environment in the lung, which could make the host vulnerable to a secondary fungal infection. Our work shows that defects in phagolysosome maturation in neutrophils and monocytes after IAV infection impair the ability of these cells to kill *A. fumigatus*, thus leading to increased fungal germination and growth and subsequent invasive aspergillosis. Our work lays a foundation for future mechanistic studies examining the exact immune modulatory events occurring in the respiratory tract after viral infection leading to secondary fungal infections.

Editor Liise-anne Pirofski, Albert Einstein College of Medicine

Address correspondence to Joshua J. Obar, Joshua.J.Obar@dartmouth.edu, or Robert A. Cramer, Robert.A.Cramer.Jr@dartmouth.edu.

The authors declare no conflict of interest.

This article is a direct contribution from Robert A. Cramer, a Fellow of the American Academy of Microbiology, who arranged for and secured reviews by Chad Steele, Tulane University, and Floyd Wormley, Jr., Texas Christian University.

Received 13 October 2022
Accepted 17 October 2022
Published 15 November 2022

KEYWORDS *Aspergillus fumigatus*, influenza A virus, superinfection, invasive pulmonary aspergillosis, phagocytosis, phagolysosome maturation, pathogenesis, host-pathogen interactions, antifungal immunity, innate immunity, phagolysosome, monocytes, neutrophils

Aspergillus fumigatus is a filamentous fungus that can be commonly found in the environment. In the immunocompetent host, hundreds to thousands of *Aspergillus* conidia can be inhaled every day without disease development. The innate immune system, including macrophages, neutrophils, monocytes, and dendritic cells (DCs), recognizes fungal conidia through pattern recognition receptors (PRRs) leading to their elimination through phagocytosis and killing via reactive oxygen species (ROS) and ROS-independent mechanisms (1). However, when the immune system is impaired, inhaled conidia germinate, become pathogenic, and contribute to multiple diseases collectively termed aspergillosis. Chronic pulmonary colonization with *A. fumigatus* can lead to allergic bronchopulmonary aspergillosis (ABPA), most commonly found in individuals with cystic fibrosis (CF) or chronic obstructive pulmonary disorder (COPD) (2, 3). Conversely, in patients with severe impairments in innate immunity (e.g., chronic granulomatous disease [CGD], prolonged steroid treatment, or neutropenia) acute exposure to *A. fumigatus* can lead to fungal germination and growth into hyphae resulting in biofilm formation, penetration of the lung parenchyma, and systemic dissemination (4–6).

Recent clinical reports indicate that patients admitted to the intensive care unit (ICU) due to severe influenza virus infections may develop secondary fungal infections (7–10). Severe influenza virus infection is now considered a major risk factor for the development of influenza-associated invasive aspergillosis (IAPA) (11). However, the mechanistic causes leading to IAPA, especially in immunocompetent patients, remain poorly understood. The connections between a postinfluenza lung environment and susceptibility to secondary bacterial infection have been well documented (12, 13). In that setting, type I and type II interferons (IFNs) induced by influenza A virus (IAV) infection are known to enhance susceptibility to secondary bacterial infection (14). Furthermore, the postinfluenza environment also affects innate immune cell accumulation and function within the lungs. Specifically, neutrophils and macrophages in the postinfluenza environment have decreased phagocytosis and clearance of bacterial pathogens (15, 16). Taken together, these results demonstrate that innate immune responses observed in the postinfluenza environment lead to defective antibacterial innate immune clearance, which can drive vulnerability to secondary bacterial infections, but the involvement of alterations in the susceptivity to secondary fungal infection remains unresolved. Recent results from a murine model of IAPA suggest that the elevated IFN production post-IAV infection induces STAT1 signaling and inhibits neutrophil recruitment, which leads to IAPA (17). However, a comprehensive study examining innate immune cell function and antifungal immunity following IAV infection is needed to define the cause(s) of IAPA development in these IAV-infected hosts.

In our current study, we established a murine IAV-*A. fumigatus* (IAV-*Af*) superinfection model that we used to examine the modulation of the antifungal innate immune response within the post-IAV lung environment. As expected, mice from the IAV-*Af* superinfection group exhibited higher morbidity and mortality, fungal biofilm formation, and increased fungal burden in the lungs. We further observe that normal inflammatory immune cell recruitment occurs in the post-IAV lung environment, yet there is a significant impairment in fungal phagocytosis and killing *in vivo*. The defective killing of *A. fumigatus* observed in pulmonary neutrophils and monocytes after IAV infection is due in part to defective phagolysosome maturation. Therefore, our findings demonstrate that modulation of neutrophil and monocyte function in a post-IAV environment contributes to defective fungal clearance, leading to disease development and eventual mortality of the host.

RESULTS

Influenza A virus infection increases susceptibility to invasive pulmonary aspergillosis in mice. To understand why influenza-infected immunocompetent hosts are more susceptible to invasive pulmonary aspergillosis (IPA), we developed an IAV-*Af* superinfection model with immunocompetent mice. C57BL/6J mice were first challenged intranasally with either phosphate-buffered saline (PBS) or a sublethal dose of IAV PR/8/34 H1N1 (100 50% egg infective dose [EID_{50}]). Six days later, mice were challenged oropharyngeally with either PBS or 3.4×10^7 *A. fumigatus* CEA10 conidia for an additional 8 to 36 h (Fig. 1A). C57BL/6J mice first inoculated with IAV and then inoculated with *A. fumigatus* (IAV-*Af* superinfection) had significantly more mortality than mice challenged with IAV only or *A. fumigatus* only. In the IAV-*Af* superinfection group, mice succumbed to infection as early as 1 day post-*A. fumigatus* inoculation, with 100% mortality observed by 5 days post-fungal challenge (Fig. 1B). Increased mortality coincided with higher fungal burden in the lungs of the IAV-*Af*-superinfected group compared to the *A. fumigatus*-only infection group (Fig. 1C). Based on our experimental design, most of the IAV would be cleared by the host at the time we collected the lung samples for viral load (day 7.5 post-IAV infection), but interestingly, the quantification of the influenza viral load by quantitative reverse transcription-PCR (qRT-PCR) showed an even lower virus load in the IAV-*Af* superinfection group compared to the IAV single-infection group, indicating functional antiviral immunity in the superinfection group (Fig. 1D). To assess the development of IAPA in our mouse model, we examined lung sections with Grocott-Gomori methenamine silver (GMS) and hematoxylin and eosin (H&E) staining for fungal burden and immune cell recruitment, respectively. While most of the inoculated *A. fumigatus* cells remained as conidia at 2 days postinoculation in the *A. fumigatus*-only infection group, in the IAV-*Af* superinfection group, we observed that *A. fumigatus* conidia had germinated significantly, even forming biofilms at the infection foci (Fig. 1E). These data demonstrate that the respiratory environment found after IAV infection results in defective restriction of *A. fumigatus* germination, which correlated with the development of IAPA in our IAV-*Af* superinfection model.

Postinfluenza immunity does not affect immune cell recruitment during infection with the highly virulent *A. fumigatus* CEA10 strain. Host innate immunity, which is largely mediated by neutrophils, macrophages, and dendritic cells, plays important roles in preventing IPA (18–23). Quantitative deficiency in any of these immune cells can limit fungal recognition and/or inhibition of conidial germination and fungal clearance. H&E staining indicates that substantial inflammatory immune cell accumulation occurs in the infection site of both the *A. fumigatus*-only and IAV-*Af* superinfection groups, suggesting a robust cellular innate immune response is occurring even in the post-IAV lung environment (Fig. 1F). Since a previous study indicated STAT1-dependent inhibition of neutrophil recruitment in the postinfluenza environment (17), we next asked whether there were any differences in composition and/or absolute number of the infiltrating immune cells in our IAV-*Af* superinfection model. We leveraged multiple immune staining panels (see Table S1 and Fig. S1 to S3 in the supplemental material) for flow cytometry analysis to examine the lung cellularity in our IAV-*Af* superinfection model (24). At 36 hours post-*A. fumigatus* challenge, we observed equivalent numbers of total lung cells, neutrophils ($Ly6G^+$ $CD11b^+$), monocytes ($CD11b^{hi}$ $CD64^-$ major histocompatibility complex class II [MHC-II]$^-$), and type 2 conventional dendritic cells (cDC2s) ($CD103^-$ $CD11b^+$) in both the *A. fumigatus*-only infection and IAV-*Af* superinfection groups that were increased compared to the those of the PBS control and IAV single-infection groups (Fig. 2A, B, E, and G). We also observed equivalent increases in interstitial macrophages ($CD11b^{hi}$ $CD64^+$) and plasmacytoid DCs (pDCs) ($CD317^+$) in both the IAV-only infection and IAV-*Af* superinfection groups compared to the PBS control (Fig. 2D and H). We also examined the cellular composition by calculating the percentage of each cell type (Fig. S4). Similar to cell number observations, both the *A. fumigatus*-only infection and IAV-*Af* superinfection groups had a significant increase in the percentage of neutrophils in the leukocyte population compared to PBS controls,

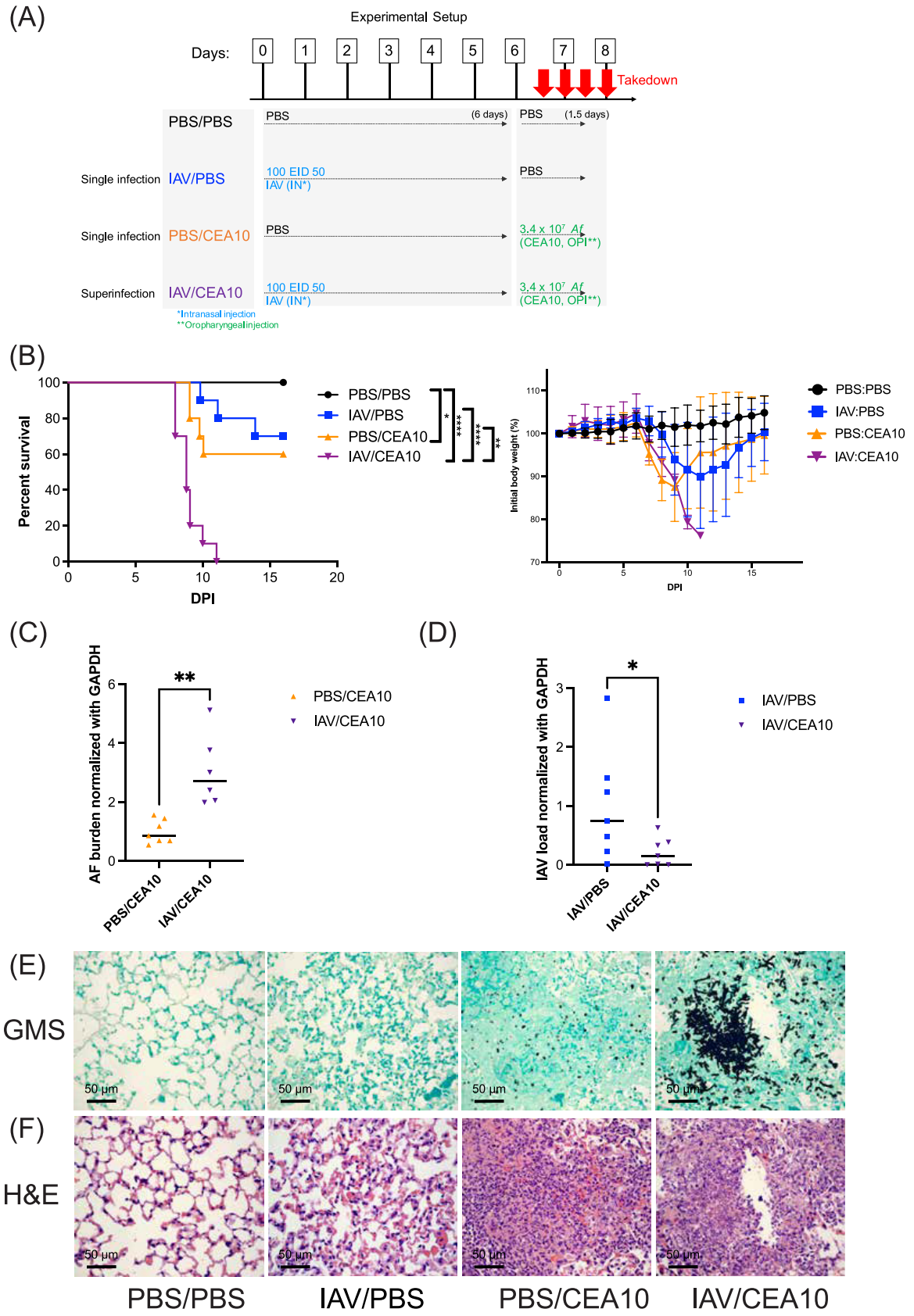

FIG 1 Influenza A virus infection aggravates invasive aspergillosis disease progression. (A) Schematic design of IAV-*Af* infection mouse model. C57BL/6J mice were inoculated with 100 EID_{50} of A/PR/8/34 (IAV) or PBS at day 0 followed by 3.4 × 10^7 CEA10 conidia or PBS at

(Continued on next page)

and there was no difference between those two experimental groups (Fig. S4A). We observe an increased percentage of interstitial macrophages and pDC populations in the IAV-only infection group compared to the *A. fumigatus*-only infection and IAV-*Af* superinfection groups, although there was no difference in total cell numbers (Fig. S4C and G). Collectively, our flow cytometry analysis results suggest that the recruitment of multiple immune cell types to the lung following IAV infection and *A. fumigatus* infection still contributes to coresponsive cell recruitment in the IAV-*Af* superinfection environment.

Neutrophils and monocytes in the postinfluenza lung environment have defects in antifungal killing mechanisms. Since we did not observe any differences in either the absolute numbers of innate immune cells or their compositions, we hypothesized that the lung environment after IAV infection results in altered antifungal effector function(s) within the recruited innate immune cells. This seemed likely, since defects in innate immune cell function, rather than recruitment, can lead to IPA development in corticosteroid-treated patients and mice (25, 26). In order to test this hypothesis, we utilized the fluorescent *Aspergillus* reporter (FLARE) assay to quantify both the uptake and viability of *A. fumigatus* conidia within specific immune cell types in the murine lungs (Fig. S5) (27). Thirty-six hours postinoculation of Alexa Fluor 633 (AF633)-labeled monomeric red fluorescent protein (mRFP)-labeled CEA10 (FLARE) conidia, both neutrophils (Fig. 3A) and monocytes (Fig. 3B) showed a slight decrease in conidial uptake, with an almost 2-fold increase in conidial viability within the IAV-*Af* superinfection group compared to *A. fumigatus*-only infection. In contrast, we observed no differences in conidial uptake or viability within alveolar macrophages (Fig. 3C) or interstitial macrophages (Fig. 3D). Within cDC2 cells, we observed a very minor decrease in conidial uptake, but no change in conidial viability (Fig. 3E). Besides the increase in intracellular viability of *A. fumigatus* in neutrophils and monocytes, we also noticed that the remaining extracellular conidia showed higher viability in the single-cell suspension from murine lungs in the FLARE assay (Fig. 3G). In parallel, single-cell lung suspensions showed an almost 2-fold increase in fungal CFU from the IAV-*Af* superinfection group compared to the *A. fumigatus*-only infection group (Fig. 3F), which corroborates our observations with the FLARE assay. Collectively, these data suggest that both neutrophils and monocytes have defects in their antifungal phagocytotic and killing processes in the post-IAV environment, which could explain why *A. fumigatus* can germinate, grow, and form biofilms in the post-IAV lung environment ultimately leading to the development of disease.

Neutrophils and monocytes induce ROS production normally in the post-IAV lung environment. ROS production by innate leukocytes plays an important role in controlling pathogen growth, particularly *Staphylococcus aureus* and *A. fumigatus*, as highlighted by infections in patients with X-linked chronic granulomatous disease (28, 29) and mice lacking NADPH oxidase components (30). Previous studies observed that impaired ROS production by innate immune cells is associated with decreased fungal killing and phagocytotic function (21). Therefore, we hypothesized that neutrophils and monocytes in the post-IAV lung environment were impaired in their ability to induce ROS production. To test this hypothesis using the IAV-*Af* superinfection model, we isolated immune cells from infected mice and incubated them with the cellular dye CM-H2DCFDA [5-(and-6)-chloromethyl-2′,7′-dichlorodihydrofluorescein diacetate] to detect total ROS production by both neutrophils and monocytes. We then determined both the

FIG 1 Legend (Continued)
day 6. Mice were euthanized at either 8, 24, 36, or 48 h post-CEA10 inoculation. (B) Survival curve (left) of mice with PBS inoculation, IAV single infection, CEA10 single infection, and IAV-CEA10 superinfection ($n = 10$) and the weights (right) of mice in each group. Two independent experiments were performed, and data are shown as the representative results. (C) For quantification of pathogen load, RNA was isolated from the lungs of mice exposed to 6 days of either IAV or PBS followed by 36 h of CEA10 or PBS inoculation. Fungal burden was examined by qRT-PCR on *A. fumigatus* 18S rRNA ($n = 7$). (D) Viral load was examined by qRT-PCR on viral matrix protein ($n = 7$). Panels C and D are representative of three independent experiments. (E) For lung histology, mice were euthanized after 6 days of IAV or PBS incubation followed by 48 h postinoculation with CEA10 or PBS. Representative histology images of mice lungs were observed with (E) GMS staining and (F) H&E staining. Two independent experiments were performed with $n = 5$ per experiment. The log rank test and Gehan-Breslow-Wilcoxon test were performed for statistical analysis of the survival curve, and nonparametric analyses were performed (Mann-Whitney for single comparisons) for the pathogen load. All error bars represent standard deviations. NS, not significant at $P > 0.05$; *, $P \leq 0.05$; **, $P \leq 0.01$; ***, $P \leq 0.001$; ****, $P \leq 0.0001$.

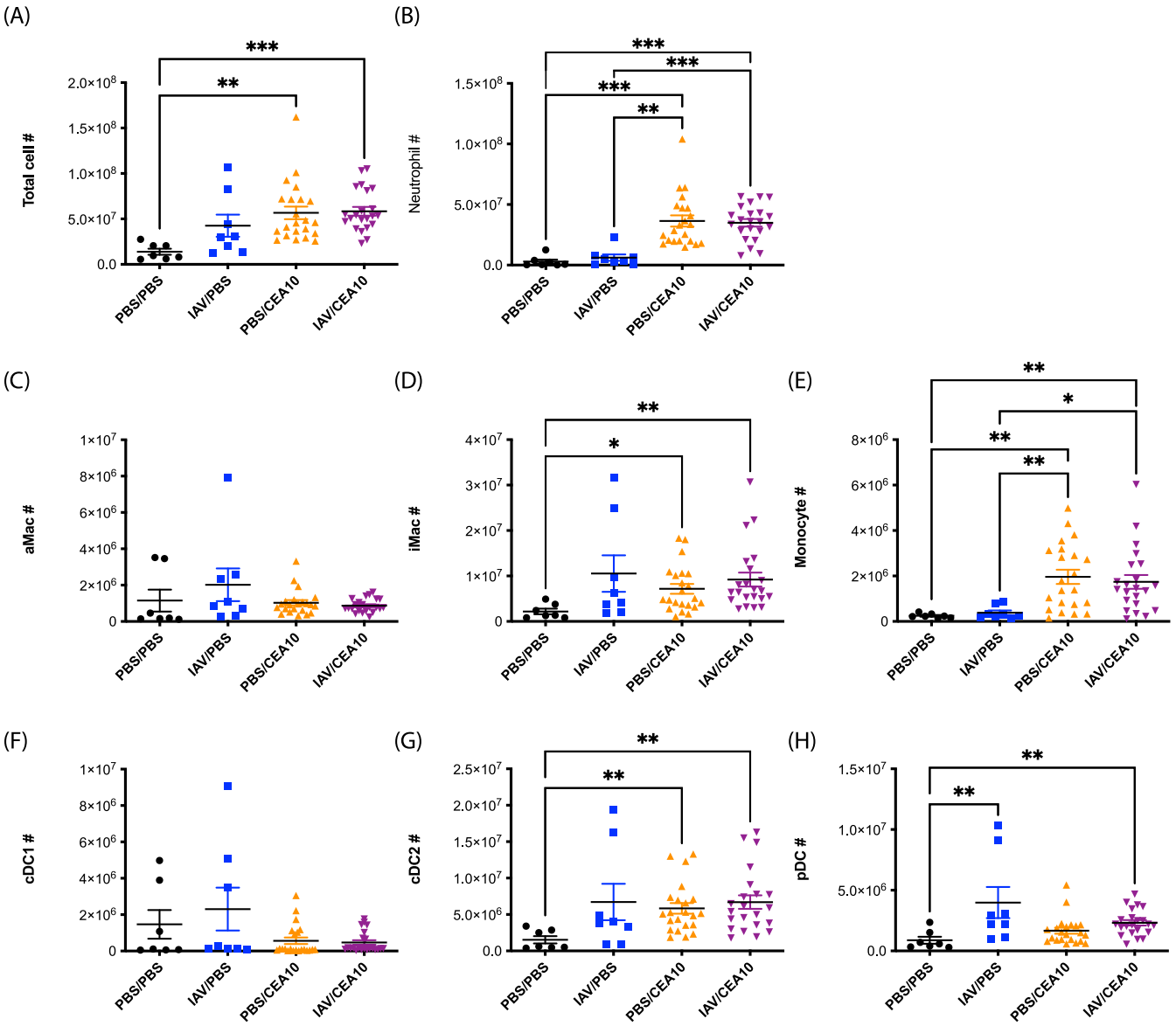

FIG 2 Influenza A virus infection does not affect lung cellularity during *A. fumigatus* infection. C57BL/6J mice were inoculated with 100 EID_{50} of A/PR/8/34 (IAV) or PBS at day 0 followed by 3.4 × 10^7 CEA10 conidia or PBS at day 6. Mice were euthanized at 36 h postinoculation with CEA10 or PBS for lung cellularity experiments. Three independent experiments were performed, and data are shown as the combined results (PBS/PBS group, $n = 7$; IAV/PBS group, $n = 8$; PBS/CEA10 group, $n = 22$; IAV/CEA10 group, $n = 22$). All lung cell numbers were acquired by flow cytometry as indicated: (A) total lung cells, (B) neutrophils ($CD45^+$ $Ly6G^+$ $CD11b^+$), (C) alveolar macrophages (aMac) ($Ly6G^-$ $CD103^-$ $SiglecF^+$ $CD11b^+$), (D) interstitial macrophages (iMac) ($Ly6G^-$ $CD103^-$ $SiglecF^-$ $CD11b^{hi}$ $CD64^+$), (E) monocytes ($Ly6G^-$ $CD103^-$ $SiglecF^-$ $CD11b^{hi}$ $CD64^-$ MHC-II^-), (F) $CD103^+$ cDC1s (MHC-II^+ $CD11c^+$ $CD11b^-$ $CD103^+$), (G) $CD11b^+$ cDC2s (MHC-II^{hi} $CD11c^{hi}$ $CD103^-$ $CD11b^+$), (H) pDCs (MHC-II^+ $CD11c^+$ $CD11b^-$ $CD103^-$ $CD317^+$). The Kruskal-Wallis test with Dunn's multiple comparisons was performed for statistical analyses. All error bars represent standard deviations. NS, not significant at $P > 0.05$; *, $P \leq 0.05$; **, $P \leq 0.01$; ***, $P \leq 0.001$; ****, $P \leq 0.0001$.

percentage of cells with a positive signal from CM-H2DCFDA as well as the amount of ROS produced on a per cell basis. We chose to examine the ROS response during early fungal infection since increased fungal germination and growth were observed by 24 h post-*A. fumigatus* infection. To do this, we collected lung cells at 8 h post-*A. fumigatus* infection. We observed increased ROS production in neutrophils and monocytes from both *A. fumigatus*-only infection and IAV-*Af* superinfection groups compared to both the PBS control and IAV-only infection groups. Furthermore, we observed no decrease in ROS production from the neutrophils and monocytes from the IAV-*Af* superinfection group compared to the *A. fumigatus*-only infection, suggesting that the fungus-induced ROS burst was not impaired in the post-IAV lung environment (Fig. 4A and B). For the

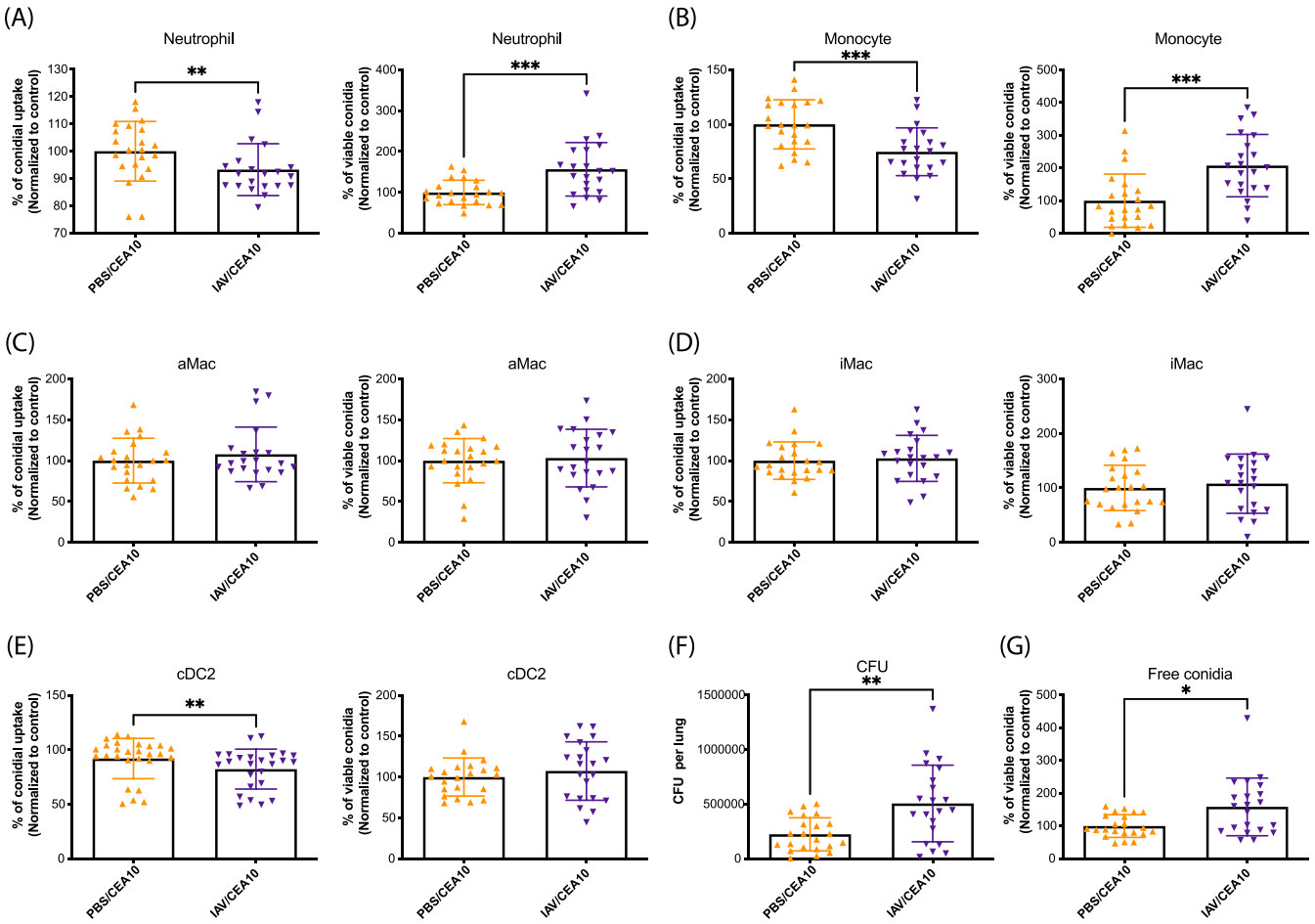

FIG 3 Defects in leukocyte-mediated fungal killing post-influenza A virus infection. C57BL/6J mice were inoculated with 100 EID_{50} of A/PR/8/34 (IAV) or PBS at day 0 followed by 3.4×10^7 FLARE ($mRFP^+/AF633^+$) conidia or PBS at day 6. Mice were euthanized at 36 h postinoculation with FLARE conidia or PBS. The percentage of cells positive for conidial tracer ($AF633^+$) and conidial viability within the immune cells ($mRFP^+/AF633^+$) were analyzed. Phagocytosis and conidial viability were examined in (A) neutrophils ($CD45^+$ $Ly6G^+$ $CD11b^+$), (B) monocytes ($Ly6G^-$ $CD103^-$ $SiglecF^-$ $CD11b^{hi}$ $CD64^-$ $MHC\text{-}II^-$), (C) alveolar macrophages (aMac) ($Ly6G^-$ $CD103^-$ $SiglecF^+$ $CD11b^+$), (D) interstitial macrophages (iMac) ($Ly6G^-$ $CD103^-$ $SiglecF^-$ $CD11b^{hi}$ $CD64^+$), and (E) $CD11b^+$ cDC2s ($MHC\text{-}II^{hi}$ $CD11c^{hi}$ $CD103^-$ $CD11b^+$). (F) The viability of FLARE conidia within immune cells in the lung suspension was assessed by CFU. (G) The viability of free FLARE conidia in the lung suspension is shown as the percentage of $mRFP^+$ cells in the free conidial population ($AF633^+$ FSC^{low} SSC^{low}). Three independent experiments were performed, and data are shown as the combined results (PBS/CEA10 group, $n = 22$; IAV/CEA10 group, $n = 21$). The Mann-Whitney test with single comparisons was performed. All error bars represent standard deviations. NS, not significant at $P > 0.05$; *, $P \leq 0.05$; **, $P \leq 0.01$; ***, $P \leq 0.001$; ****, $P \leq 0.0001$.

percentage of cells that produced ROS, we observed an increased percentage in IAV-induced neutrophils and *A. fumigatus*-induced monocytes, but there was no significant difference between the IAV- or *A. fumigatus*-only infection and IAV-*Af* superinfection groups (Fig. S7A and B). Our data demonstrate that neutrophils and monocytes are still capable of significant ROS production during early *A. fumigatus* infection in the post-IAV environment, indicating a defect in ROS production from these two critical innate immune cells is not likely responsible for the development of disease in our model.

Phagolysosome maturation is impaired in neutrophils and monocytes found in the post-IAV lung environment. Rapid maturation of the phagosome through LC3-associated phagocytosis and subsequent phagosome maturation to the phagolysosome is necessary for antifungal killing and control of *A. fumigatus* germination and growth (31, 32). Since ROS production was not impaired by neutrophils and monocytes isolated from the post-IAV lung environment, we next hypothesized that defects in phagolysosome maturation within leukocytes from the IAV-*Af* superinfection contributes to the impaired antifungal killing. To test this hypothesis, we quantified phagolysosome maturation using pHrodo Green zymosan bioparticle (pHrodo-zymosan) staining in the neutrophils and monocytes 8 h after *A. fumigatus* challenge. We determined the

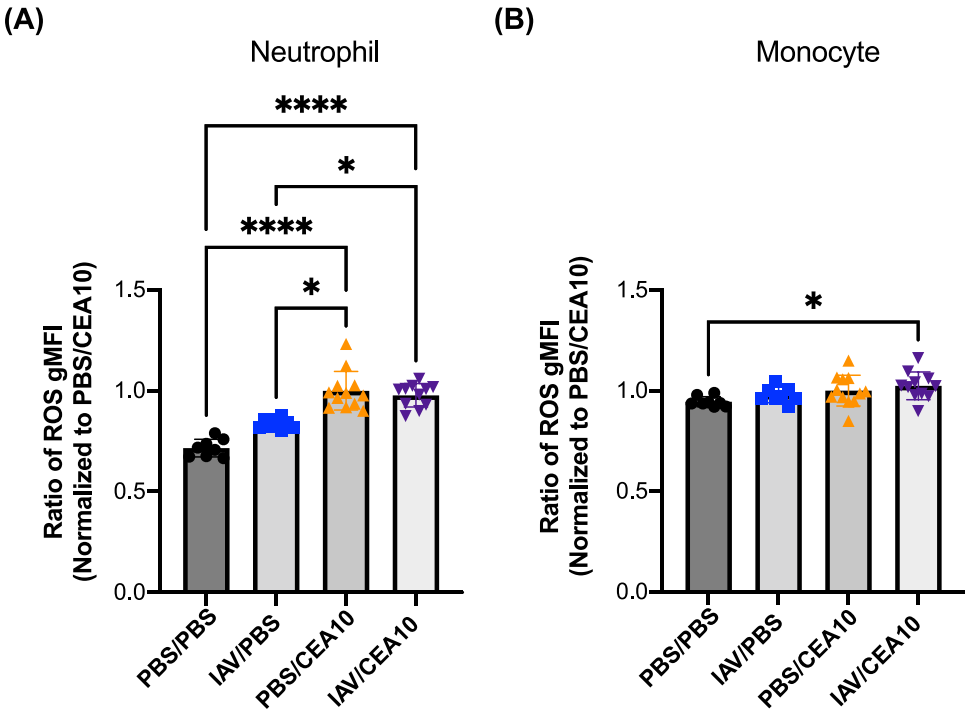

FIG 4 Postinfluenza immunity does not hinder neutrophil or monocyte ROS production. C57BL/6J mice were inoculated with 100 EID_{50} of A/PR/8/34 (IAV) or PBS at day 0 followed by 3.4×10^7 CEA10 conidia or PBS at day 6. Mice were euthanized at 8 h postinoculation with CEA10 or PBS for ROS measurement. Lung cell suspensions were stained with CM-H2DCFDA for 30 min and then stained for neutrophils and monocytes. ROS production was measured by the signal from CM-H2DCFDA staining in (A) neutrophils ($Ly6G^+$) and (B) monocytes ($Ly6G^-$ $SiglecF^-$ $CD11b^{hi}$ $CD64^-$ $MHC\text{-}II^-$). Two independent experiments were performed, and data are shown as the combined results (PBS/PBS group, $n = 8$; IAV/PBS group, $n = 8$; PBS/CEA10 group, $n = 12$; IAV/CEA10 group, $n = 11$). The Kruskal-Wallis test with Dunn's multiple comparisons was performed for statistical analyses. All error bars represent standard deviations. NS, not significant at $P > 0.05$; *, $P \leq 0.05$; **, $P \leq 0.01$; ***, $P \leq 0.001$; ****, $P \leq 0.0001$.

percentage of active cells by the percentage of cells with a positive signal from a color change of pHrodo-zymosan and the number of mature phagolysosomes in these active cells by the intensity of their pHrodo-zymosan signal. In our murine model, both neutrophils and monocytes from the IAV-only infection group had significant reductions in their pHrodo-zymosan signal from mature phagolysosomes compared to the PBS control (Fig. 5A and B). Similar to our observation in the IAV-only infection group, we also observed reduced signal from mature phagolysosomes in neutrophils and monocytes from the IAV-*Af* superinfection group compared to the PBS control (Fig. 5A and B). These data suggest that the post-IAV lung environment significantly impacts phagolysosome maturation in neutrophils and monocytes, which correlates with the impaired intracellular killing ability against fungal conidia we observed in the IAV-*Af* superinfection group in the FLARE experiment (Fig. 3).

To check for the proportion of cells that are still capable of responding to fungal PAMPs in the post-IAV environment, we examined the percentage of cells with a mature phagolysosome. We observed that the percentages of lung neutrophils with mature phagolysosomes from the *A. fumigatus*-only infection and IAV-*Af* superinfection groups were reduced compared to those in the PBS controls, but there was no difference between the IAV-*Af* superinfection and either of the single-infection groups (Fig. S8A). Intriguingly, lung monocytes from the IAV-only infection and IAV-*Af* superinfection groups showed reduced mature phagolysosome-containing cells in the population compared with both the PBS control and *A. fumigatus*-only infection groups (Fig. S8B). To further test the connection between the phagolysosome maturation defect and conidial killing in the nonexhausted neutrophils from the post-IAV environment, we combined

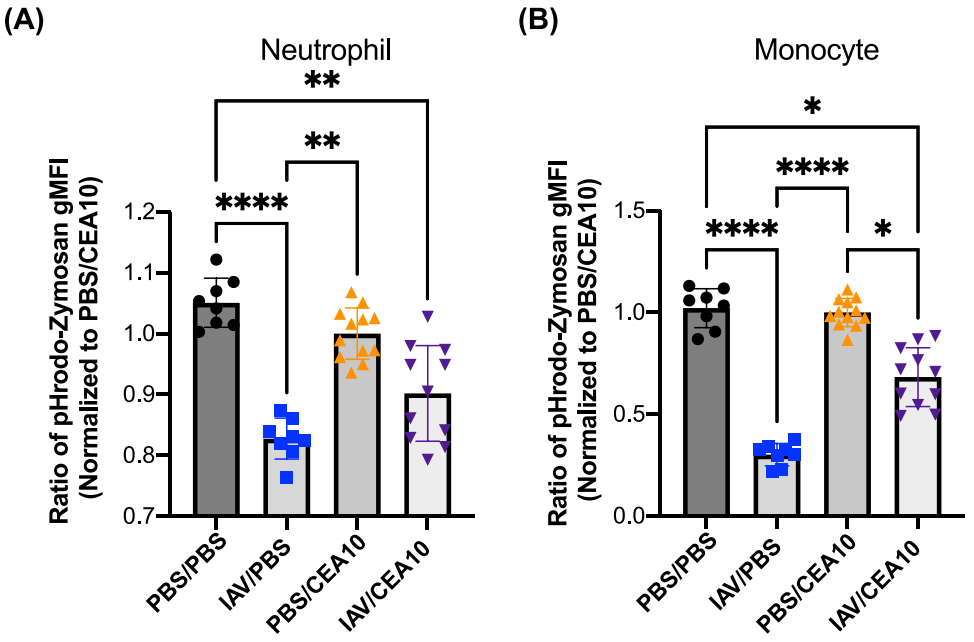

FIG 5 Reduced phagolysosome maturation can be detected in neutrophils and monocytes during early viral infection. C57BL/6J mice were inoculated with 100 EID_{50} of A/PR/8/34 (IAV) or PBS at day 0 followed by 3.4×10^7 CEA10 conidia or PBS at day 6. Mice were euthanized at 8 h postinoculation with CEA10 or PBS for phagolysosome maturation analysis. Lung cell suspensions were incubated with pHrodo-zymosan for 2 h and then stained for neutrophils and monocytes. The phagolysosome maturation level was measured by the signal from the color change of pHrodo-zymosan in (A) neutrophils ($Ly6G^+$) and (B) monocytes ($Ly6G^-$ $SiglecF^-$ $CD11b^{hi}$ $CD64^-$ $MHC\text{-}II^-$). Two independent experiments were performed, and data are shown as the combined results (PBS/PBS group, $n = 8$; IAV/PBS group, $n = 8$; PBS/CEA10 group, $n = 12$; IAV/CEA10 group, $n = 11$). The Kruskal-Wallis test with Dunn's multiple comparisons was performed for statistical analyses. All error bars represent standard deviations. NS, not significant at $P > 0.05$; *, $P \leq 0.05$; **, $P \leq 0.01$; ***, $P \leq 0.001$; ****, $P \leq 0.0001$.

the FLARE experiment with pHrodo-zymosan staining in our animal model. With confocal imaging, we observed $Ly6G^+$ neutrophils containing mature phagolysosome signal as well as live or dead conidia (Fig. 6A). The presence of pHrodo-$zymosan^+$ neutrophils in the lung from IAV-*Af* superinfection mice suggests these neutrophils were still functional in the post-IAV environment (Fig. 6B). However, these pHrodo-$zymosan^+$ neutrophils had less mature phagolysosome signal (Fig. 6C) and show decreased conidial killing (Fig. 6E). Collectively, these data suggest that neutrophils and monocytes in the post-IAV environment are impaired in phagolysosome maturation (Fig. 5), which correlates with decreased fungal killing (Fig. 3) and increased fungal burden (Fig. 1).

Increased inflammation but decreased PRR gene expression in the IAV-*Af* superinfection environment. In order to investigate the potential upstream pathway(s) contributing to defective phagolysosome maturation and fungal clearance we saw in the IAV-*Af* superinfection model, we utilized qRT-PCR of antifungal genes in RT^2 Profiler PCR arrays (PAMM-147ZD) with immune cell RNA from lungs of mice challenged with *A. fumigatus* only and IAV-*Af* superinfection. At 8 h post-*A. fumigatus* challenge, we found increased mRNA levels for *Nlrp3*, *Pycard*, *Ptgs2*, *Cd36*, *Cxcl10*, *Nfkb1*, *Mapk14*, and *Ccr5* and decreased mRNA levels for *Il10*, *Il2*, and *Jun* in the IAV-*Af* superinfection group compared to mice challenged only with *A. fumigatus* (Fig. 7). Interestingly, despite an enhanced inflammatory environment under IAV-Af superinfection conditions, which likely reflects the increased fungal growth, we observed a decrease in the mRNA levels of *Tlr9*, *Scarf1*, and *Colec12*, as well as *Irak4*, which is involved in myddosome and Toll-like receptor 9 (TLR9) signaling (Fig. 7). Our data reveal that while IAV-*Af* superinfected mice have a robust inflammatory response, there is a specific decrease in PRR mRNA levels that could alter the early host-fungus interaction and drive the impaired phagolysosome maturation and antifungal killing observed in neutrophils and monocytes. Future studies will

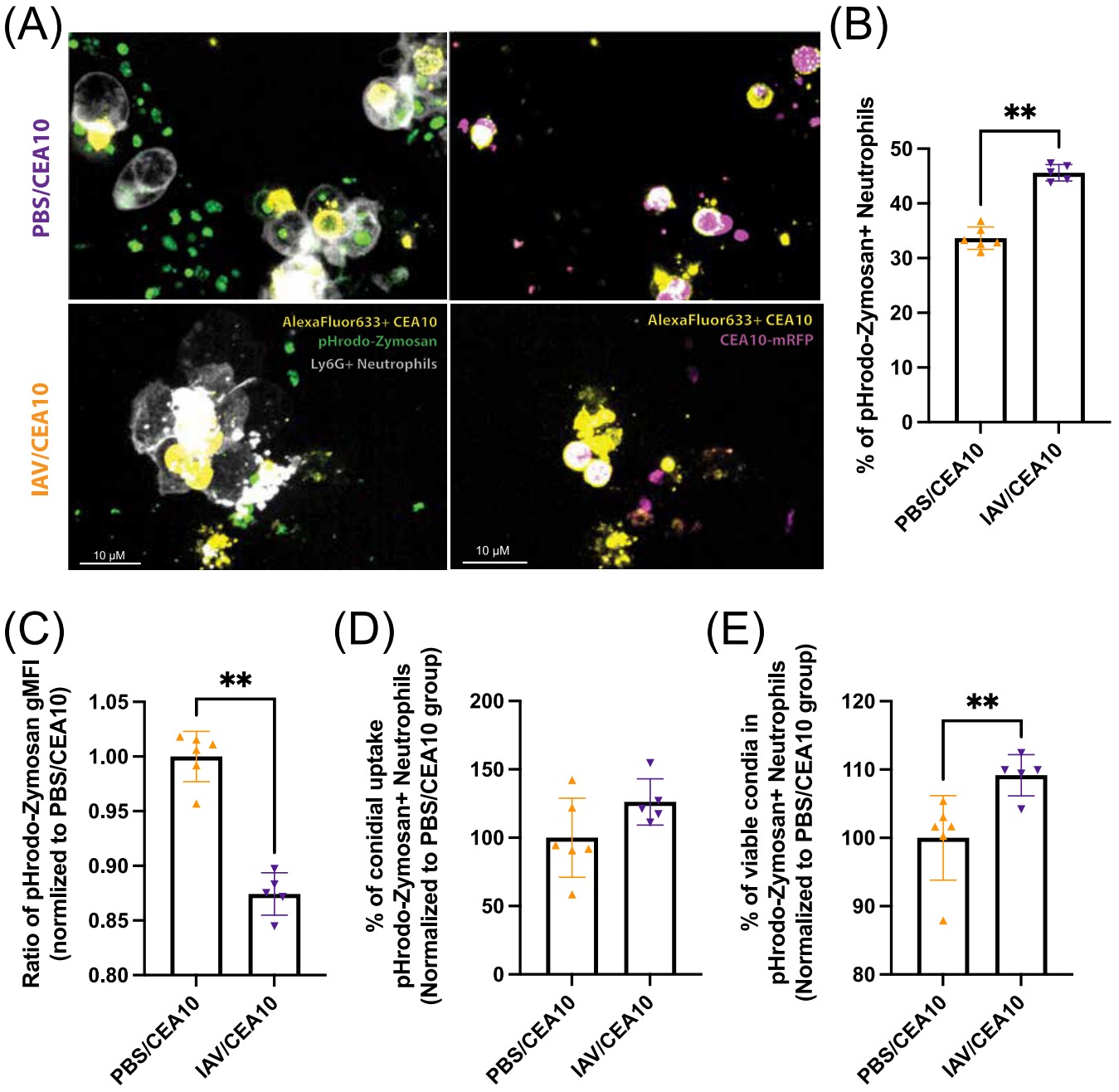

FIG 6 Functional neutrophils from the post-IAV environment show decreasing phagolysosome maturation and conidial killing. C57BL/6J mice were inoculated with 100 EID_{50} of A/PR/8/34 (IAV) or PBS at day 0 followed by 3.4×10^7 FLARE ($mRFP^+/AF633^+$) conidia or PBS at day 6. Mice were euthanized at 36 h postinoculation with FLARE conidia or PBS. Lung cell suspensions were incubated with pHrodo-zymosan for 2 h and then stained for neutrophils. (A) Representative confocal images of neutrophil labeling (Ly6G-Pb [white]), mature phagolysosome (pHrodo-zymosan [green]), labeled conidia (AF633 [yellow]), and conidial viable marker (mRFP [pink]). The right images feature labeled conidia, neutrophils, and pHrodo-zymosan signal. The left images feature labeled conidia and RFP to indicate fungal viability. Fungal conidia with no RFP signal are considered "dead." (B) Currently functional neutrophils are indicated as pHrodo-zymosan$^+$ cells. (C) The number of mature phagolysosomes is shown by the geometric mean fluorescent intensity (gMFI) of pHrodo-zymosan in $Ly6G^+$ pHrodo-zymosan$^+$ cells. The percentage of cells positive for conidia ($AF633^+$) and conidial viability within the immune cells ($mRFP^+/AF633^+$) were analyzed as (D) the percentage of conidial uptake in $Ly6G^+$ pHrodo-Zymosan$^+$ cells and (E) the percentage of viable conidia in $Ly6G^+$ pHrodo-zymosan$^+$ cells. This repeated experiment was done as the combination of FLARE experiment (Fig. 3) and phagolysosome maturation measurement (Fig. 5) (PBS/CEA10 group, $n = 6$; IAV/CEA10 group, $n = 5$). The Mann-Whitney test with single comparisons was performed. All error bars represent standard deviations. NS, not significant at $P > 0.05$; *, $P \leq 0.05$; **, $P \leq 0.01$; ***, $P \leq 0.001$; ****, $P \leq 0.0001$.

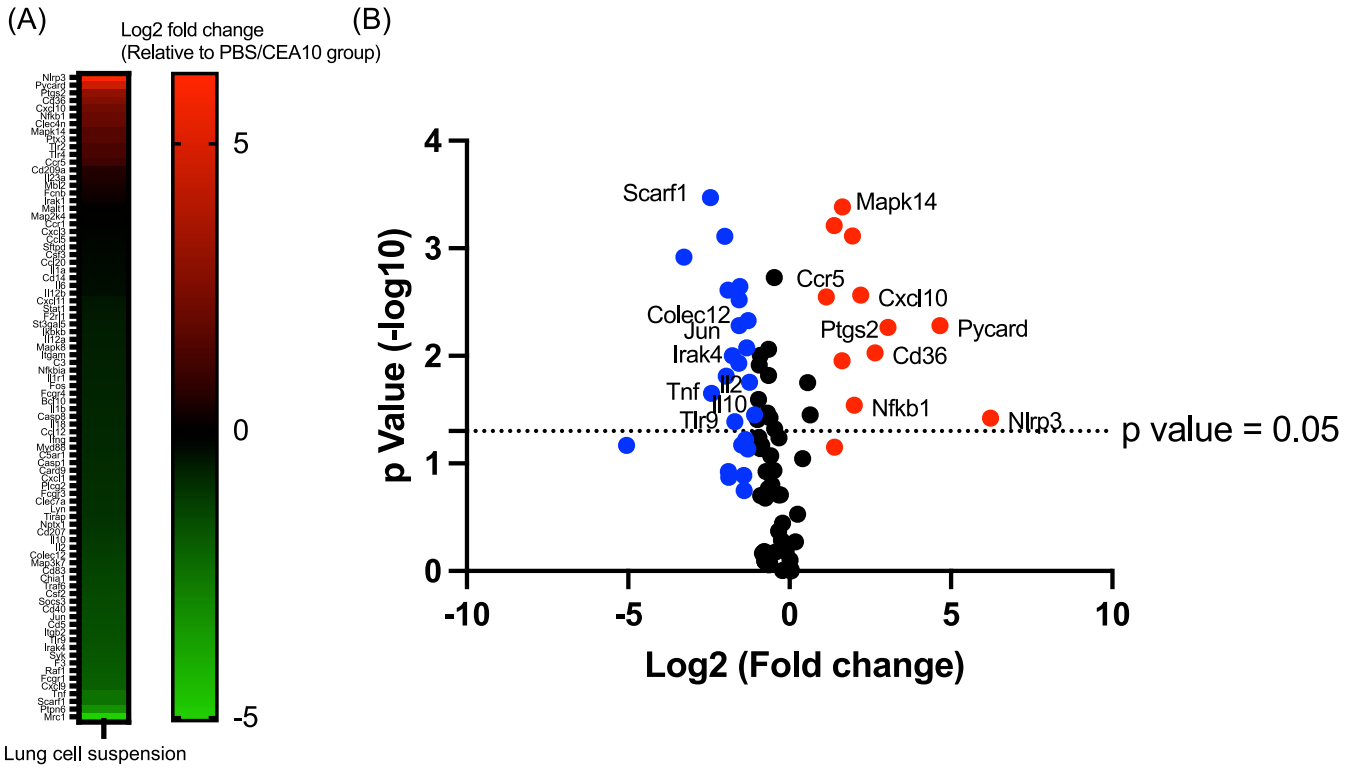

FIG 7 Influenza A virus infection increases transcripts of genes associated with an inflammatory response but reduces transcript levels of known fungal pattern recognition receptors. C57BL/6J mice were inoculated with 100 EID_{50} of A/PR/8/34 (IAV) or PBS at day 0 followed by 3.4×10^7 CEA10 conidia or PBS at day 6. Mice were euthanized at 8 h postinoculation with CEA10 or PBS for antifungal gene transcript analysis. Antifungal gene transcript levels were measured by qRT-PCR with RNA from lung cell suspensions. (A) Increased (red) or decreased (green) transcript levels of genes associated with antifungal responses in the IAV/CEA10 group compared to the PBS/CEA10 group are represented by the heat map (PBS/CEA10 group, $n = 3$; IAV/CEA10 group, $n = 3$). (B) A volcano plot shows the distribution of fold changes of antifungal gene transcript levels in the IAV/CEA10 group compared to the PBS/CEA10 group. Genes with an increase in fold changes of >2 are shown in red, and genes with a decrease in fold changes of >2 are shown in blue. The *P* value threshold of 0.05 (Student's *t* test) is indicated by the line in the plot.

seek to explore the mechanism(s) underlying this virus-induced defect in phagolysosome maturation in the presence of *A. fumigatus* conidia.

DISCUSSION

Seasonal influenza infection is a common annual respiratory disease among humans, and 1 to 2% of patients with symptomatic illness require hospitalization in the United States (33). Of those hospitalized, ~5 to 10% progress to ICU admission (34). Patients in the ICU due to severe IAV infections are well known to develop secondary bacterial infections, but in recent years the incidence of secondary fungal infections has been reported with a prevalence of IAPA between 5 and 19% and a mortality rate of ~50% (7, 8, 35, 36). Importantly, both immunocompromised and immunocompetent individuals in the ICU were at risk for developing IAPA (35). Moreover, this does not seem to be isolated to severe respiratory infection with IAV, because recent clinical case reports from the current severe acute respiratory syndrome coronavirus 2 (SARS-CoV2) pandemic suggest that secondary fungal infections are observed in patients with severe COVID-19 (37–39). COVID-19-associated pulmonary aspergillosis (CAPA) is reported in 20 to 35% of cases in recent reports from Europe (37). Thus, severe respiratory viral infection is an emerging risk factor for invasive aspergillosis and warrants further mechanistic studies.

Influenza infection can cause epithelial cell damage and leakage, induce antiviral cytokine production, impair further inflammatory cellular recruitment, and impair the phagocytic and antimicrobial activity of macrophages and neutrophils, which can all contribute to the increased risk of developing secondary bacterial infection (12, 13). However, there is a significant knowledge gap in understanding how IAV infection makes the lung environment conducive for fungal growth leading to the development

of IAPA. Recently, in a human retrospective observational study, Feys et al. identified a couple breaches in antifungal immunity in patients with IAPA and CAPA that included decreased integrity of the epithelial barrier, decreased antifungal cytokine expression (e.g., gamma interferon [IFN-γ]), and decreased gene expression for pathways involved in fungal phagocytosis and killing mainly mediated by neutrophils (38). One major hurdle to understanding virus-induced pulmonary aspergillosis has been the lack of experimental models to dissect secondary fungal infection. Our work here, together with the model from Robinson and colleagues (17), has established a robust IAV-*Af* superinfection mouse model that can be used for future mechanistic studies. To this end, we used our new model to determine whether prior IAV infection created a favorable environment for fungal escape from the host antifungal innate immune response, and if so, to experimentally define the host cellular function(s) modulated by the post-IAV lung environment.

Host resistance against *A. fumigatus* can be lost by either quantitative or qualitative defects in the antifungal leukocyte response (39). To begin to investigate how prior IAV infection enhanced susceptibility to *A. fumigatus*, we examined both inflammatory immune cell accumulation in the lungs and their antifungal functions in that environment. Flow cytometry analysis of lung suspensions showed that levels of neutrophil, interstitial macrophage, monocyte, and cDC2 accumulation in the lung parenchyma were similar in IAV-*Af*-superinfected and *A. fumigatus*-only-infected mice (Fig. 2). This is in line with the inferred cellular makeup of the human IAPA bronchoalveolar lavage fluid in human patients with IAPA versus IAV infection alone (38). In contrast, Tobin et al. previously found that the proportion of neutrophils and alveolar macrophages was decreased in IAV-*Af*-superinfected mice compared to *A. fumigatus*-only infection (17). The authors did not quantify absolute numbers of inflammatory cells but did note overall increased inflammation in their histological analysis, which could explain our discrepant results. Additionally, our studies utilized the CEA10 strain of *A. fumigatus*, while Tobin et al. used the ATCC 42202 strain (17), which could also drive the differences in our findings since *A. fumigatus* strain heterogeneity alters virulence and host immune responses (40–45). Future studies will examine the role of *A. fumigatus* strain heterogeneity in driving IAPA.

Since we observed no obvious quantitative differences in the innate immune cell response in the IAV-*Af*-superinfected mice versus mice infected with *A. fumigatus* only, it was likely that the innate immune cells from the IAV-*Af*-superinfected mice had functional defects in their antifungal effector response in the post-IAV lung environment. To examine the overall antifungal effector functions of host leukocytes in our murine IAV-*Af* superinfection model, we used the robust *in vivo* FLARE method to determine both conidial uptake and killing by professional phagocytes in the presence or absence of IAV infection (27). We found that neutrophils and monocytes had defects in both conidial uptake and killing in the post-IAV lung environment (Fig. 3). This is in line with what others have observed with regard to leukocyte function in IAV-induced secondary bacterial infections (16, 46). Moreover, this directly supports the transcriptome correlates identified in human patients with IAPA (38).

Innate immune resistance against *A. fumigatus* requires both ROS-dependent and ROS-independent mechanisms for fungal conidial clearance (39, 47). Oxidative stress from host ROS production is known for preventing fungal conidial germination (48). IAV infection can limit ROS production in neutrophils and monocytes after secondary bacterial challenge (49). In contrast, to what was seen with bacterial challenge, we observed no defect in ROS production by both neutrophils and monocytes from IAV-*Af*-superinfected mice compared to mice infected with only *A. fumigatus* (Fig. 4). We also noticed that there were more ROS-producing neutrophils in IAV single infection, which was consistent with previous IAV infection studies (49, 50). Thus, our data suggest that monocytes and neutrophils from IAV-*Af*-superinfected mice maintain robust ROS production in response to secondary fungal challenge, which may be reflective of

bacterial infections being highly dependent on TLRs for the induction of ROS, whereas fungal infections are highly dependent on CLRs for the induction of ROS.

ROS-independent conidial clearance in both macrophages and neutrophils requires phagolysosome maturation to create an acidic environment, which is necessary for conidial killing (51, 52). A recent study also showed that betacoronavirus infection can lead to lysosome destruction, affect its acidification, and reduce bacterial clearance in the macrophage (53). To assess phagolysosome maturation in the neutrophils and monocytes within the IAV-*Af*-superinfected lungs, we used pHrodo-zymosan staining. Both neutrophils and monocytes displayed a significant reduction in pHrodo-zymosan signal following both IAV infection alone or IAV-*Af* superinfection (Fig. 5), which is supportive of impaired or slowed phagolysosome maturation in the post-IAV lung environment. In addition to the phagolysosome maturation level, we also examined the percentage of cells that are still able to take up and send the pHrodo-zymosan into mature phagolysosomes through the percentage of pHrodo-zymosan-positive cells in neutrophil and monocyte populations. Interestingly, we observed a significant reduction of monocytes that can respond to and send pHrodo-zymosan into mature phagolysosomes in the post-IAV environment. This suggests that the defects are in both pathogen-associated molecular pattern (PAMP) responsiveness and phagolysosome maturation in the post-IAV environment for monocytes (Fig. S8B). However, we did not detect a significant reduction in the percentage of pHrodo-zymosan$^+$ neutrophils from IAV-infected mice, indicating potential differences between neutrophils and monocytes in the post-IAV environment. Instead, the significant reduction of pHrodo-zymosan uptake in both the *A. fumigatus* single-infection and IAV-*Af* superinfection groups might be due to potential neutrophil exhaustion during fungal infection since the pHrodo-zymosan uptake requires the recognition and binding to the Dectin-1 receptor (Fig. S8A). Still, we can detect a decrease in mature phagolysosome and conidial killing in the pHrodo-zymosan$^+$ neutrophils, suggesting that the phenotype is not contributed by cell exhaustion post-IAV infection (Fig. 6C and E). In summary, our data revealed that the post-IAV environment does not inhibit immune cell recruitment or ROS production in the face of a highly virulent *A. fumigatus* strain, but specifically reduces phagolysosome maturation in neutrophils and monocytes, which can lead to conidial escape from the host innate immunity during fungal infection.

A major question remaining from our study is how the post-IAV lung environment impairs phagolysosome maturation. To investigate the upstream signal that may drive defective fungal clearance in the IAV-*Af* superinfection mice in our model, we examined antifungal gene expression in isolated immune cells. Based on viral-bacterial superinfection literature, we expected to observe an anti-inflammatory gene expression profile after IAV infection and during early fungal infection (53–56). However, we observed that immune cells from IAV-*Af* superinfection mice displayed increased inflammatory gene transcript levels and decreased anti-inflammatory cytokine gene transcript levels (Fig. 7), indicating enhanced immune responses during early fungal infection. This result may be due to the increase in fungal burden in the superinfection group. Interestingly, we found reduced expression of three PRR genes (*Tlr9*, *Scarf1*, and *Colec12*) (Fig. 7). TLR9 is known to be recruited to the *A. fumigatus*-containing phagosome and contribute to fungus-induced immune cell activation (54, 55). On the other hand, TLR9 trafficking to the phagosome is mediated by Dectin-1 signaling and phagolysosome maturation and acidification (56, 57). Although we did not observe a difference in *Clec7a* transcript levels in the IAV-*Af* superinfection mice compared to the *A. fumigatus*-only infection group, the decreased *Tlr9* expression and reduced phagosome acidification in our IAV-*Af* superinfection model suggest impaired TLR9 activation and signaling. In addition to decreased *Tlr9* expression, we also observed decreased *Irak4* expression (Fig. 7), which is a component of the myddosome needed for TLR-dependent signaling (58). Therefore, it is likely that reduction of TLR9 signaling contributes to defects in phagolysosome maturation in neutrophils and monocytes or vice versa.

LC3-associated phagocytosis (LAP) is known to be associated with more rapid phagolysosome maturation (59). LAP is known to be essential for host resistance against *A.*

fumigatus (31, 32). In human IAPA and CAPA patients, genes *MAP1LC3B* and *SQSTM1*, related to LAP were decreased, while *CDC20*, the gene encoding for the CDC20 protein which is involved in LC3 degradation, was upregulated in the superinfection group comparing to viral single infection (38). Following CpG oligonucleotide activation of TLR9, LC3 can be recruited to the signaling endosome and mediate IKKα recruitment that leads to TRAF3 and IRF7 activation (60). Additionally, IFN-γ enhances LAP following *A. fumigatus* challenge, but in humans with IAPA, the levels of IFN-γ are diminished compared to those in infections with IAV only (38). Thus, we hypothesize that reducing TLR9 signaling in our IAV-*Af* superinfection model contributes to a decrease in LAP, further linking phagolysosome maturation and *A. fumigatus* clearance (32). This link between phagosome maturation and effective fungal clearance is well supported by mechanistic studies in other fungal pathogens, where phagolysosome maturation is key to clearance of infection (61–63). Still, further investigation of the role of LAP components specifically and contributions of TLR9 signaling in our IAV-*Af* superinfection model is required to address this possibility and to assess whether therapeutically targeting this pathway could restore host resistance against *A. fumigatus* after IAV infection.

In conclusion, we found that the post-IAV lung environment negatively affects phagolysosome maturation, which corresponds to reduced antifungal killing by both neutrophils and monocytes. This reduction in fungal killing leads to increased fungal germination, fungal growth, and eventual establishment of IAPA. Further studies are needed to investigate the upstream signals altering phagolysosome maturation in the presence of IAV. More information could be leveraged therapeutically to restore antifungal activity of impaired neutrophils and monocytes after IAV infection, to enhancing fungal clearance and clinical outcomes in IAPA patients. The findings from this study are also more broadly applicable, as recent clinical case reports have revealed that patients with severe COVID-19 can develop a secondary infection with *A. fumigatus* and these patients had worse clinical outcomes and higher mortality. It remains to be determined what the underlying mechanisms are for SARS-CoV2-induced secondary *A. fumigatus* infection.

MATERIALS AND METHODS

Animal inoculation. C57BL/6J mice between 8 and 10 weeks old were purchased from Jackson Laboratories. Mice were housed in autoclaved cages at ≤4 mice per cage with a supply of HEPA-filtered air and water. Only mice with a weight under 22 g were selected for all experiments. The stock of influenza A/PR/8/34 H1N1 was purchased from Charles River, and the titer of the virus was quantified by 50% egg infectious dose (EID_{50}). *A. fumigatus* strain CEA10 (also called CBS144.89) was grown on a 1% glucose minimal medium (GMM) plate for 3 days at 37°C. The conidia were collected in 0.01% Tween 20 and washed 3 times with sterile PBS. Mice were infected with 100 EID_{50} of influenza A/PR/8/34 H1N1 (in 50 μL sterile PBS) or control PBS by intranasal instillation under isoflurane anesthesia. After 6 days of viral infection, mice were infected with 3.4×10^7 CEA10 conidia (in 100 μL sterile PBS) or control PBS by oropharyngeal instillation. Mice were then euthanized between 8 to 48 h post-*Aspergillus* challenge. Animals were monitored daily for disease symptoms, and we carried out our animal studies in strict accordance with the recommendations in the *Guide for the Care and Use of Laboratory Animals* (64). The animal experimental protocol (no. 00002167) was approved by the Institutional Animal Care and Use Committee (IACUC) at Dartmouth College.

RNA preparation and pathogen quantification. Mice were inoculated with either PBS, influenza A/PR/8/34 H1N1, or CEA10 as described previously, and the lungs were removed at euthanasia for RNA extraction. Lungs were flash frozen, lyophilized, and homogenized with glass beads using a Mini-Beadbeater (BioSpec Products, Inc., Bartlesville, OK) and resuspended in TRIzol reagent (Thomas Scientific) and chloroform to extract RNA according to the manufacturer's instructions. Five micrograms of RNA was treated with Ambion Turbo DNase (Life Technologies) according to the manufacturer's instructions. One microgram of DNase-treated RNA was further processed with a QuantiTech reverse transcription kit with an additional 0.5 ng of random decamer. The amounts of RNA were normalized to *Gapdh* for fungal and viral burden. For murine GAPDH (glyceraldehyde-3-phosphate dehydrogenase), the following primers were used: forward, 5′-TCATCCCAGAGCTGAACG-3′; reverse, 5′-GGGAGTTGCTGTT GAAGTC-3′. The fungal burden was measured by qRT-PCR on *Aspergillus fumigatus* 18S rRNA. For fungal burden, the following primers and probe were used: forward primer, 5′-GGCCCTTAAATAGCCCGGT-3′; reverse primer, 5′-TGAGCCGATAGTCCCCCTAA-3′; TaqMan probe, AGCCAGCGGCCCGCAAATG. The viral load was measured by qRT-PCR on viral matrix protein (17). For viral load, the following primers and probe were used: forward primer, 5′-GGACTGCAGCGTAGACGCTT-3′; reverse primer, 5′-CATCCTGTTGT ATATGAGGCCCAT-3′; PrimeTime probe, 5′-56-FAM (carboxyfluorescein)-CTCAGTTAT-ZEN-TCTGCTGGT GCACTTGCCA-3IABkFQ-3′.

Histology staining. Mice were inoculated with either PBS, influenza A/PR/8/34 H1N1, or CEA10 as described previously and euthanized at 48 h post-fungal inoculation. After euthanasia, cannulas were inserted into the trachea and the lungs were removed from the body cavity. The lungs were inflated and immersed in 10% buffered formalin phosphate for 24 h and stored in 70% ethanol until embedding. Paraffin-embedded sections were stained with hematoxylin and eosin (H&E) to observe inflammation and Grocott-Gomori methenamine silver (GMS) to observe fungi. The images of H&E and GMS slides were analyzed microscopically with a Zeiss Axioplan 2 imaging microscope (Carl Zeiss Microimaging, Inc., Thornwood, NY) fitted with a QImaging Retiga-SRV Fast 1394 RGB camera.

Flow cytometry: lung cellularity and fluorescence *Aspergillus* reporter analysis. For the fluorescence *Aspergillus* reporter (FLARE) experiments, the CEA10 conidia that expressed mRFP were generated by ectopically insertion of a *gpdA*-driven mRFP construct with the *ptrA* gene as selection marker. To generate FLARE conidia, conidia that expressed mRFP were collected and labeled with Alexa Fluor 633 as described previously (27). Mice were inoculated with either PBS, influenza A/PR/8/34 H1N1, or FLARE conidia as described previously and euthanized at 36 h post-fungal inoculation. To harvest the single-cell suspension from mouse lungs, the whole lungs were minced and digested in buffer containing 2.2 mg/mL collagenase type IV (Worthington), 1 U/mL DNase 1 (New England Biotech), and 5% fetal bovine serum (FBS) at 37°C for 45 min. The digested samples were passed through 18-gauge needle, incubated in red blood cell (RBC) lysis buffer (eBioScience), neutralized in PBS, passed through 100-μm-pore filter, and counted. The antibodies used for the flow cytometry analysis of different populations were as follows. For the neutrophil population, lung cells were stained with Survival dye (efluor780; eBioScience), CD45 (Pacific Orange; Invitrogen), CD64 (BV421; BioLegend), Ly6G conjugated with fluorescein isothiocyanate (FITC) (BioLegend), and CD11b conjugated with peridinin chlorophyll protein ([PerCP]) and Cy5.5 (BioLegend). For the macrophage/monocyte population, lung cells were stained with Survival dye (efluor780; eBioScience), IA/IE (MHC-II) (BV605; BioLegend), SiglecF (BV421; BD BioScience), Ly6G-FITC (BioLegend), CD103-FITC (BioLegend), CD11b-PerCP-Cy5.5 (BioLegend), and CD64 conjugated with phycoerythrin (PE)-Cy7 (BioLegend). For DC populations, lung cells were stained with Survival dye (efluor780; eBioScience), IA/IE (MHC-II) (BV605; BioLegend), CD11b (Pacific Blue; BioLegend), CD103-FITC (BioLegend), CD317-PerCP-Cy5.5 (BioLegend), and CD11c-PE-Cy7 (BioLegend). The gating strategies for each of the cell populations are indicated in Fig. S1 to S3 in the supplemental material. The data were collected by Beckman Coulter Cytoflex S and analyzed with FlowJo version 10.8.1.

To quantify fungal CFU of intracellular conidia, lung cells in the single-cell suspension were further homogenized with glass beads using Mini-Beadbeater (BioSpec Products, Inc., Bartlesville, OK) and resuspended in PBS. The samples were diluted 1:100 and then plated on 1/2 Sabouraud dextrose agar plates, incubated overnight, and counted for CFU.

Immune cell function: intracellular ROS production and phagolysosome maturation. Mice were inoculated with either PBS, influenza A/PR/8/34 H1N1, or CEA10 conidia as described previously and euthanized at 8 h post-fungal inoculation. The single-cell suspensions were harvested as described previously. For measurement of intracellular ROS, lung cells from the single-cell suspensions were incubated with 1 μM CM-H2DCFDA [5-(and-6)-chloromethyl-2′,7′-dichlorodihydrofluorescein diacetate] (Thermo) at 37°C for 30 min according to the manufacturer's instructions. For the measurement of phagolysosome maturation, lung cells were incubated with 0.05 mg/mL of pHrodo Green zymosan bioparticles (Invitrogen) at 37°C for 2 h according to the manufacturer's instructions. CM-H2DCFDA or pHrodo-zymosan-stained lung cells were then stained with Survival dye (efluor780; eBioScience), IA/IE (MHC-II) (BV605, BioLegend), SiglecF (BV421; BD BioScience), Ly6G-PE (BioLegend), CD11b-PerCP-Cy5.5 (BioLegend), and CD64-PE-Cy7 (BioLegend) for the gating of neutrophils and monocytes. The gating strategies for each of the cell populations are indicated in Fig. S6. To confirm intracellular localization of signals by microscopy and verify flow cytometry results in Fig. 6, mice were inoculated with CEA10-mRFP FLARE conidia, and lung cells were incubated with 0.05 mg/mL of pHrodo-zymosan at 37°C for 2 h and stained with Survival dye (efluor780; eBioScience) and Ly6G-Pb (BioLegend) or Ly6G-Pb (BioLegend) alone. Images were acquired using an Andor W1 spinning disk confocal microscope mounted with a Nikon Eclipse Ti inverted microscope stand. Lasers with wavelengths of 405 nm (Ly6G-Pb; BioLegend), 488 nm (pHrodo-zymosan; Invitrogen), 561 nm (CEA10-mRFP) and 633 nm (Alexa Fluor 633-labeled conidia) (Invitrogen) were used for excitation. Images were viewed using Fiji software and were used to visualize flow cytometry results. Flow cytometry data were collected by Beckman Coulter Cytoflex S and analyzed with FlowJo version 10.8.1.

RNA preparation and antifungal gene expression evaluation. Mice were inoculated with either PBS, influenza A/PR/8/34 H1N1, or CEA10 conidia as described previously and euthanized at 8 h post-fungal inoculation. The single-cell suspensions were harvested as described previously. Following the cell isolation, the cells were lysed and RNA was collected with an RNeasy kit according to the manufacturer's instruction (Qiagen). A 0.5-μg sample of RNA was further processed with the RT^2 First Strand kit (Qiagen). cDNA was mixed with RT2 SYBR green master mix (Qiagen) and loaded onto RT^2 Profiler PCR arrays containing primers for antifungal genes (PAMM-147ZD; Qiagen) (Table S2). The RNA load was normalized with *Actb*, *Gapdh*, and *Hsp90ab1*.

Statistical analysis. All statistical analyses were performed with Prism 9.3.0 software (GraphPad Software, Inc., San Diego, CA). The log rank test and Gehan-Breslow-Wilcoxon test were performed for statistical analysis of the survival curve. For animal experiments, nonparametric analyses were performed (Kruskal-Wallis with Dunn's multiple comparisons and Mann-Whitney test with single comparisons). All error bars represent standard deviations, and significance is noted as follows: NS, not significant at $P > 0.05$; *, $P \leq 0.05$; **, $P \leq 0.01$; ***, $P \leq 0.001$; ****, $P \leq 0.0001$.

SUPPLEMENTAL MATERIAL

Supplemental material is available online only.

FIG S1, TIF file, 1 MB.
FIG S2, TIF file, 1 MB.
FIG S3, TIF file, 1.1 MB.
FIG S4, TIF file, 0.5 MB.
FIG S5, TIF file, 1.4 MB.
FIG S6, TIF file, 1.4 MB.
FIG S7, TIF file, 0.3 MB.
FIG S8, TIF file, 0.4 MB.
TABLE S1, TIF file, 0.9 MB.
TABLE S2, XLSX file, 0.01 MB.

ACKNOWLEDGMENTS

We give special thanks to Eric Dufour of the Center for Comparative Medicine and Research (CCMR) staff for helping with the animal experiments. Flow cytometry data were collected with technical assistance and resources from the Immune Monitoring and Flow Cytometry Resource (IMFCSR) at the Norris Cotton Cancer Center at Dartmouth.

This project was supported by NIH/NIAID grant R21-AI152019 (J.J.O.), NIH/NIAID R01AI39632 (R.A.C.), and a Cystic Fibrosis Foundation Research Development Grant (STANTO15RO). M.S.G. was supported by the Dartmouth College Immunology Training Program (NIH/NIAID T32 AI007363). We also thank the Imaging Facility at Dartmouth (Ann Lavanway) and the Biomolecular Targeting Core (P20-GM113132) for use of equipment.

REFERENCES

1. Margalit A, Kavanagh K. 2015. The innate immune response to Aspergillus fumigatus at the alveolar surface. FEMS Microbiol Rev 39:670–687. https://doi.org/10.1093/femsre/fuv018.
2. Kauffman HF. 2003. Immunopathogenesis of allergic bronchopulmonary aspergillosis and airway remodeling. Front Biosci 8:190–196. https://doi.org/10.2741/990.
3. Pashley CH. 2014. Fungal culture and sensitisation in asthma, cystic fibrosis and chronic obstructive pulmonary disorder: what does it tell us? Mycopathologia 178:457–463. https://doi.org/10.1007/s11046-014-9804-y.
4. Dagenais TRT, Keller NP. 2009. Pathogenesis of Aspergillus fumigatus in invasive aspergillosis. Clin Microbiol Rev 22:447–465. https://doi.org/10.1128/CMR.00055-08.
5. El-Baba F, Gao Y, Soubani AO. 2020. Pulmonary aspergillosis: what the generalist needs to know. Am J Med 133:668–674. https://doi.org/10.1016/j.amjmed.2020.02.025.
6. King J, Henriet SSV, Warris A. 2016. Aspergillosis in chronic granulomatous disease. J Fungi 2:15. https://doi.org/10.3390/jof2020015.
7. Schwartz IS, Friedman DZP, Zapernick L, Dingle TC, Lee N, Sligl W, Zelyas N, Smith SW. 2020. High rates of influenza-associated invasive pulmonary aspergillosis may not be universal: a retrospective cohort study from Alberta, Canada. Clin Infect Dis 71:1760–1763. https://doi.org/10.1093/cid/ciaa007.
8. Zou P, Wang C, Zheng S, Guo F, Yang L, Zhang Y, Liu P, Shen Y, Wang Y, Zhang X, Tang L, Gao H, Li L. 2020. Invasive pulmonary aspergillosis in adults with avian influenza A (H7N9) pneumonia in China: a retrospective study. J Infect Dis 221(Suppl 2):S193–S197. https://doi.org/10.1093/infdis/jiz682.
9. Rouzé A, Lemaitre E, Martin-Loeches I, Povoa P, Diaz E, Nyga R, Torres A, Metzelard M, Du Cheyron D, Lambiotte F, Tamion F, Labruyere M, Geronimi CB, Luyt C-E, Nyunga M, Pouly O, Thille AW, Megarbane B, Saade A, Magira E, Llitjos J-F, Ioannidou I, Pierre A, Reignier J, Garot D, Kreitmann L, Baudel J-L, Voiriot G, Plantefeve G, Morawiec E, Asfar P, Boyer A, Mekontso-Dessap A, Makris D, Vinsonneau C, Floch P-E, Marois C, Ceccato A, Artigas A, Gaudet A, Nora D, Cornu M, Duhamel A, Labreuche J, Nseir S, coVAPid Study Group. 2022. Invasive pulmonary aspergillosis among intubated patients with SARS-CoV-2 or influenza pneumonia: a European multicenter comparative cohort study. Crit Care 26:11. https://doi.org/10.1186/s13054-021-03874-1.
10. Ku YH, Chan KS, Yang CC, Tan CK, Chuang YC, Yu WL. 2017. Higher mortality of severe influenza patients with probable aspergillosis than those with and without other coinfections. J Formos Med Assoc 116:660–670. https://doi.org/10.1016/j.jfma.2017.06.002.
11. Rijnders BJA, Schauwvlieghe AFAD, Wauters J. 2020. Influenza-associated pulmonary aspergillosis: a local or global lethal combination? Clin Infect Dis 71:1764–1767. https://doi.org/10.1093/cid/ciaa010.
12. McCullers JA. 2014. The co-pathogenesis of influenza viruses with bacteria in the lung. Nat Rev Microbiol 12:252–262. https://doi.org/10.1038/nrmicro3231.
13. Jia L, Xie J, Zhao J, Cao D, Liang Y, Hou X, Wang L, Li Z. 2017. Mechanisms of severe mortality-associated bacterial co-infections following influenza virus infection. Front Cell Infect Microbiol 7:338. https://doi.org/10.3389/fcimb.2017.00338.
14. Barman TK, Racine R, Bonin JL, Califano D, Salmon SL, Metzger DW. 2021. Sequential targeting of interferon pathways for increased host resistance to bacterial superinfection during influenza. PLoS Pathog 17:e1009405. https://doi.org/10.1371/journal.ppat.1009405.
15. Abramson JS, Lewis JC, Lyles DS, Heller KA, Mills EL, Bass DA. 1982. Inhibition of neutrophil lysosome-phagosome fusion associated with influenza virus infection in vitro. Role in depressed bactericidal activity. J Clin Invest 69:1393–1397. https://doi.org/10.1172/jci110580.
16. Sun K, Metzger DW. 2008. Inhibition of pulmonary antibacterial defense by interferon-γ during recovery from influenza infection. Nat Med 14:558–564. https://doi.org/10.1038/nm1765.
17. Tobin JM, Nickolich KL, Ramanan K, Pilewski MJ, Lamens KD, Alcorn JF, Robinson KM. 2020. Influenza suppresses neutrophil recruitment to the lung and exacerbates secondary invasive pulmonary aspergillosis. J Immunol 205:480–488. https://doi.org/10.4049/jimmunol.2000067.
18. Bonnett CR, Cornish EJ, Harmsen AG, Burritt JB. 2006. Early neutrophil recruitment and aggregation in the murine lung inhibit germination of Aspergillus fumigatus conidia. Infect Immun 74:6528–6539. https://doi.org/10.1128/IAI.00909-06.
19. Mircescu MM, Lipuma L, van Rooijen N, Pamer EG, Hohl TM. 2009. Essential role for neutrophils but not alveolar macrophages at early time points following Aspergillus fumigatus infection. J Infect Dis 200:647–656. https://doi.org/10.1086/600380.

20. Schaffner A, Douglas H, Braude AI, Davis CE. 1983. Killing of Aspergillus spores depends on the anatomical source of the macrophage. Infect Immun 42:1109–1115. https://doi.org/10.1128/iai.42.3.1109-1115.1983.
21. Philippe B, Ibrahim-Granet O, Prévost MC, Gougerot-Pocidalo MA, Sanchez Perez M, van der Meeren A, Latgé JP. 2003. Killing of Aspergillus fumigatus by alveolar macrophages is mediated by reactive oxidant intermediates. Infect Immun 71:3034–3042. https://doi.org/10.1128/IAI.71.6.3034-3042.2003.
22. Gafa V, Lande R, Gagliardi MC, Severa M, Giacomini E, Remoli ME, Nisini R, Ramoni C, di Francesco P, Aldebert D, Grillot R, Coccia EM. 2006. Human dendritic cells following Aspergillus fumigatus infection express the CCR7 receptor and a differential pattern of interleukin-12 (IL-12), IL-23, and IL-27 cytokines, which lead to a Th1 response. Infect Immun 74:1480–1489. https://doi.org/10.1128/IAI.74.3.1480-1489.2006.
23. Bozza S, Gaziano R, Spreca A, Bacci A, Montagnoli C, di Francesco P, Romani L. 2002. Dendritic cells transport conidia and hyphae of Aspergillus fumigatus from the airways to the draining lymph nodes and initiate disparate Th responses to the fungus. J Immunol 168:1362–1371. https://doi.org/10.4049/jimmunol.168.3.1362.
24. Misharin AV, Morales-Nebreda L, Mutlu GM, Scott Budinger GR, Perlman H. 2013. Flow cytometric analysis of macrophages and dendritic cell subsets in the mouse lung. Am J Respir Cell Mol Biol 49:503–510. https://doi.org/10.1165/rcmb.2013-0086MA.
25. Gustafson TL, Schaffner W, Lavely GB, Stratton CW, Johnson HK, Hutcheson RH. 1983. Invasive aspergillosis in renal transplant recipients: correlation with corticosteroid therapy. J Infect Dis 148:230–238. https://doi.org/10.1093/infdis/148.2.230.
26. Balloy V, Huerre M, Latgé JP, Chignard M. 2005. Differences in patterns of infection and inflammation for corticosteroid treatment and chemotherapy in experimental invasive pulmonary aspergillosis. Infect Immun 73:494–503. https://doi.org/10.1128/IAI.73.1.494-503.2005.
27. Jhingran A, Mar KB, Kumasaka DK, Knoblaugh SE, Ngo LY, Segal BH, Iwakura Y, Lowell CA, Hamerman JA, Lin X, Hohl TM. 2012. Tracing conidial fate and measuring host cell antifungal activity using a reporter of microbial viability in the lung. Cell Rep 2:1762–1773. https://doi.org/10.1016/j.celrep.2012.10.026.
28. O'Neill S, Brault J, Stasia M-J, Knaus UG. 2015. Genetic disorders coupled to ROS deficiency. Redox Biol 6:135–156. https://doi.org/10.1016/j.redox.2015.07.009.
29. Anjani G, Vignesh P, Joshi V, Shandilya JK, Bhattarai D, Sharma J, Rawat A. 2020. Recent advances in chronic granulomatous disease. Genes Dis 7:84–92. https://doi.org/10.1016/j.gendis.2019.07.010.
30. Balloy V, Chignard M. 2009. The innate immune response to Aspergillus fumigatus. Microbes Infect 11:919–927. https://doi.org/10.1016/j.micinf.2009.07.002.
31. Akoumianaki T, Kyrmizi I, Valsecchi I, Gresnigt MS, Samonis G, Drakos E, Boumpas D, Muszkieta L, Prevost MC, Kontoyiannis DP, Chavakis T, Netea MG, van de Veerdonk FL, Brakhage AA, El-Benna J, Beauvais A, Latge JP, Chamilos G. 2016. Aspergillus cell wall melanin blocks LC3-associated phagocytosis to promote pathogenicity. Cell Host Microbe 19:79–90. https://doi.org/10.1016/j.chom.2015.12.002.
32. Martinez J, Malireddi RKS, Lu Q, Cunha LD, Pelletier S, Gingras S, Orchard R, Guan JL, Tan H, Peng J, Kanneganti TD, Virgin HW, Green DR. 2015. Molecular characterization of LC3-associated phagocytosis (LAP) reveals distinct roles for Rubicon, NOX2, and autophagy proteins. Nat Cell Biol 17:893–906. https://doi.org/10.1038/ncb3192.
33. Rolfes MA, Foppa IM, Garg S, Flannery B, Brammer L, Singleton JA, Burns E, Jernigan D, Olsen SJ, Bresee J, Reed C. 2018. Annual estimates of the burden of seasonal influenza in the United States: a tool for strengthening influenza surveillance and preparedness. Influenza Other Respir Viruses 12:132–137. https://doi.org/10.1111/irv.12486.
34. Reed C, Chaves SS, Kirley PD, Emerson R, Aragon D, Hancock EB, Butler L, Baumbach J, Hollick G, Bennett NM, Laidler MR, Thomas A, Meltzer MI, Finelli L. 2015. Estimating influenza disease burden from population-based surveillance data in the United States. PLoS One 10:e0118369. https://doi.org/10.1371/journal.pone.0118369.
35. Schauwvlieghe AFAD, Rijnders BJA, Philips N, Vanderbeke L, Wauters J, van den Berg CHSB, Juffermans NP, Schauwvlieghe AFAD, Rijnders BJA, Philips N, Verwijs R, Vanderbeke L, van Tienen C, Lagrou K, Verweij PE, van de Veerdonk FL, Gommers D, Spronk P, Bergmans DCJJ, Hoedemaekers A, Andrinopoulou E-R, van den Berg CHSB, Juffermans NP, Hodiamont CJ, Vonk AG, Depuydt P, Boelens J, Wauters J. 2018. Invasive aspergillosis in patients admitted to the intensive care unit with severe influenza: a retrospective cohort study. Lancet Respir Med 6:782–792. https://doi.org/10.1016/S2213-2600(18)30274-1.
36. Vanderbeke L, Spriet I, Breynaert C, Rijnders BJA, Verweij PE, Wauters J. 2018. Invasive pulmonary aspergillosis complicating severe influenza: epidemiology, diagnosis and treatment. Curr Opin Infect Dis 31:471–480. https://doi.org/10.1097/QCO.0000000000000504.
37. Arastehfar A, Carvalho A, van de Veerdonk FL, Jenks JD, Koehler P, Krause R, Cornely OA, Perlin DS, Lass-Flörl C, Hoenigl M. 2020. COVID-19 associated pulmonary aspergillosis (CAPA)—from immunology to treatment. J Fungi 6:91–17. https://doi.org/10.3390/jof6020091.
38. Feys S, Gonçalves SM, Khan M, Choi S, Boeckx B, Chatelain D, Cunha C, Debaveye Y, Hermans G, Hertoghs M, Humblet-Baron S, Jacobs C, Lagrou K, Marcelis L, Maizel J, Meersseman P, Nyga R, Seldeslachts L, Starick MR, Thevissen K, Vandenbriele C, Vanderbeke L, Vande Velde G, van Regenmortel N, Vanstapel A, Vanmassenhove S, Wilmer A, van de Veerdonk FL, de Hertogh G, Mombaerts P, Lambrechts D, Carvalho A, van Weyenbergh J, Wauters J. 2022. Lung epithelial and myeloid innate immunity in influenza-associated or COVID-19-associated pulmonary aspergillosis: an observational study. Lancet Respir Med https://doi.org/10.1016/S2213-2600(22)00259-4.
39. Latgé JP, Chamilos G. 2019. Aspergillus fumigatus and aspergillosis in 2019. Clin Microbiol Rev 33:e00140-18. https://doi.org/10.1128/CMR.00140-18.
40. Jones JT, Liu K-W, Wang X, Kowalski CH, Ross BS, Mills KAM, Kerkaert JD, Hohl TM, Lofgren LA, Stajich JE, Obar JJ, Cramer RA. 2021. Aspergillus fumigatus strain-specific conidia lung persistence causes an allergic broncho-pulmonary aspergillosis-like disease phenotype. mSphere 6:e01250-20. https://doi.org/10.1128/mSphere.01250-20.
41. Caffrey-Carr AK, Hilmer KM, Kowalski CH, Shepardson KM, Temple RM, Cramer RA, Obar JJ. 2018. Host-derived leukotriene B_4 is critical for resistance against invasive pulmonary aspergillosis. Front Immunol 8:1984. https://doi.org/10.3389/fimmu.2017.01984.
42. Caffrey-Carr AK, Kowalski CH, Beattie SR, Blaseg NA, Upshaw CR, Thammahong A, Lust HE, Tang YW, Hohl TM, Cramer RA, Obar JJ. 2017. Interleukin 1α is critical for resistance against highly virulent Aspergillus fumigatus isolates. Infect Immun 85:e00661-17. https://doi.org/10.1128/IAI.00661-17.
43. Kowalski CH, Beattie SR, Fuller KK, McGurk EA, Tang YW, Hohl TM, Obar JJ, Cramer RA. 2016. Heterogeneity among isolates reveals that fitness in low oxygen correlates with Aspergillus fumigatus virulence. mBio 7:e01515-16. https://doi.org/10.1128/mBio.01515-16.
44. Rizzetto L, Giovannini G, Bromley M, Bowyer P, Romani L, Cavalieri D. 2013. Strain dependent variation of immune responses to A. fumigatus: definition of pathogenic species. PLoS One 8:e56651. https://doi.org/10.1371/journal.pone.0056651.
45. Rosowski EE, Raffa N, Knox BP, Golenberg N, Keller NP, Huttenlocher A. 2018. Macrophages inhibit Aspergillus fumigatus germination and neutrophil-mediated fungal killing. PLoS Pathog 14:e1007229. https://doi.org/10.1371/journal.ppat.1007229.
46. Shahangian A, Chow EK, Tian X, Kang JR, Ghaffari A, Liu SY, Belperio JA, Cheng G, Deng JC. 2009. Type I IFNs mediate development of postinfluenza bacterial pneumonia in mice. J Clin Invest 119:1910–1920. https://doi.org/10.1172/JCI35412.
47. Urban CF, Backman E. 2020. Eradicating, retaining, balancing, swarming, shuttling and dumping: a myriad of tasks for neutrophils during fungal infection. Curr Opin Microbiol 58:106–115. https://doi.org/10.1016/j.mib.2020.09.011.
48. Vethanayagam RR, Almyroudis NG, Grimm MJ, Lewandowski DC, Pham CTN, Blackwell TS, Petraitiene R, Petraitis V, Walsh TJ, Urban CF, Segal BH. 2011. Role of NADPH oxidase versus neutrophil proteases in antimicrobial host defense. PLoS One 6:e28149. https://doi.org/10.1371/journal.pone.0028149.
49. Abramson JS, Mills EL, Giebink GS, Quie PG. 1982. Depression of monocyte and polymorphonuclear leukocyte oxidative metabolism and bactericidal capacity by influenza A virus. Infect Immun 35:350–355. https://doi.org/10.1128/iai.35.1.350-355.1982.
50. Akaike T, Ando M, Oda T, Doi T, Ijiri S, Araki S, Maeda H. 1990. Dependence on O_2 generation by xanthine oxidase of pathogenesis of influenza virus infection in mice. J Clin Invest 85:739–745. https://doi.org/10.1172/JCI114499.
51. Ibrahim-Granet O, Philippe B, Boleti H, Boisvieux-Ulrich E, Grenet D, Stern M, Latgé JP. 2003. Phagocytosis and intracellular fate of Aspergillus fumigatus conidia in alveolar macrophages. Infect Immun 71:891–903. https://doi.org/10.1128/IAI.71.2.891-903.2003.
52. Gazendam RP, van Hamme JL, Tool ATJ, Hoogenboezem M, van den Berg JM, Prins JM, Vitkov L, van de Veerdonk FL, van den Berg TK, Roos D, Kuijpers TW. 2016. Human neutrophils use different mechanisms to kill

Aspergillus fumigatus conidia and hyphae: evidence from phagocyte defects. J Immunol 196:1272–1283. https://doi.org/10.4049/jimmunol.1501811.
53. Peng X, Kim J, Gupta G, Agaronyan K, Mankowski MC, Korde A, Takyar SS, Shin HJ, Habet V, Voth S, Audia JP, Chang D, Liu X, Wang L, Cai Y, Tian X, Ishibe S, Kang M-J, Compton S, Wilen CB, Dela Cruz CS, Sharma L. 2022. Coronavirus lung infection impairs host immunity against secondary bacterial infection by promoting lysosomal dysfunction. J Immunol 209:1314–1322. https://doi.org/10.4049/jimmunol.2200198.
54. Herbst S, Shah A, Mazon Moya M, Marzola V, Jensen B, Reed A, Birrell MA, Saijo S, Mostowy S, Shaunak S, Armstrong-James D. 2015. Phagocytosis-dependent activation of a TLR9-BTK-calcineurin-NFAT pathway coordinates innate immunity to Aspergillus fumigatus. EMBO Mol Med 7:240–258. https://doi.org/10.15252/emmm.201404556.
55. Kasperkovitz PV, Cardenas ML, Vyas JM. 2010. TLR9 is actively recruited to Aspergillus fumigatus phagosomes and requires the N-terminal proteolytic cleavage domain for proper intracellular trafficking. J Immunol 185:7614–7622. https://doi.org/10.4049/jimmunol.1002760.
56. Mansour MK, Tam JM, Khan NS, Seward M, Davids PJ, Puranam S, Sokolovska A, Sykes DB, Dagher Z, Becker C, Tanne A, Reedy JL, Stuart LM, Vyas JM. 2013. Dectin-1 activation controls maturation of β-1,3-glucan-containing phagosomes. J Biol Chem 288:16043–16054. https://doi.org/10.1074/jbc.M113.473223.
57. Khan NS, Kasperkovitz P v, Timmons AK, Mansour MK, Tam JM, Seward MW, Reedy JL, Puranam S, Feliu M, Vyas JM. 2016. Dectin-1 controls TLR9 trafficking to phagosomes containing β-1,3 glucan. J Immunol 196:2249–2261. https://doi.org/10.4049/jimmunol.1401545.
58. de Nardo D, Balka KR, Gloria YC, Rao VR, Latz E, Masters SL. 2018. Interleukin-1 receptor-associated kinase 4 (IRAK4) plays a dual role in myddosome formation and Toll-like receptor signaling. J Biol Chem 293:15195–15207. https://doi.org/10.1074/jbc.RA118.003314.
59. Heckmann BL, Boada-Romero E, Cunha LD, Magne J, Green DR. 2017. LC3-associated phagocytosis and inflammation. J Mol Biol 429:3561–3576. https://doi.org/10.1016/j.jmb.2017.08.012.
60. Hayashi K, Taura M, Iwasaki A. 2018. The interaction between IKKα and LC3 promotes type I interferon production through the TLR9-containing LAPosome. Sci Signal 11:eaan4144. https://doi.org/10.1126/scisignal.aan4144.
61. Vylkova S, Lorenz MC. 2014. Modulation of phagosomal pH by Candida albicans promotes hyphal morphogenesis and requires Stp2p, a regulator of amino acid transport. PLoS Pathog 10:e1003995. https://doi.org/10.1371/journal.ppat.1003995.
62. Chen R, Ji G, Ma T, Huang X, Ren H, Xi L. 2015. Role of intracellular free calcium in killing Penicillium marneffei within human macrophages. Microb Pathog 83–84:29–34. https://doi.org/10.1016/j.micpath.2015.05.001.
63. Isaac DT, Coady A, Prooyen NN, Sil A. 2013. The 3-hydroxy-methylglutaryl coenzyme A lyase HCL1 is required for macrophage colonization by human fungal pathogen Histoplasma capsulatum. Infect Immun 81:411–420. https://doi.org/10.1128/IAI.00833-12.
64. National Research Council. 2011. Guide for the care and use of laboratory animals, 8th ed. National Academies Press, Washington, DC.